

Published in final edited form as:

Nano Lett. 2012 June 13; 12(6): 2697–2704. doi:10.1021/nl2041707.

Nanowire Substrate-based Laser Scanning Cytometry for Quantitation of Circulating Tumor Cells

Sang-Kwon Lee^{1,2,*}, Gil-Sung Kim², Yu Wu¹, Dong-Joo Kim², Yao Lu¹, Minsuk Kwak¹, Lin Han¹, Jung-Hwan Hyung², Jin-Kyeong Seol², Chantal Sander¹, Anjelica Gonzalez¹, Jie Li³, and Rong Fan^{1,4,*}

¹Department of Biomedical Engineering, Yale University, New Haven, CT 06511, USA

²Department of Semiconductor Science and Technology, Chonbuk National University, Jeonju 561-756, Korea

³Department of Neuropathology, Yale School of Medicine, New Haven, CT 06520, USA

⁴Yale Comprehensive Cancer Center, New Haven, CT 06520, USA

Abstract

We report on the development of a nanowire substrate-enabled laser scanning imaging cytometry for rare cell analysis in order to achieve quantitative, automated, and functional evaluation of circulating tumor cells. Immuno-functionalized nanowire arrays have been demonstrated as a superior material to capture rare cells from heterogeneous cell populations. The laser scanning cytometry method enables large-area, automated quantitation of captured cells and rapid evaluation of functional cellular parameters (e.g. size, shape and signaling protein) at the single-cell level. This integrated platform was first tested for capture and quantitation of human lung carcinoma cells from a mixture of tumor cells and leukocytes. We further applied it to the analysis of rare tumor cells spiked in fresh human whole blood (several cells per mL) that emulate metastatic cancer patient blood and demonstrated the potential of this technology for analyzing circulating tumor cells in the clinical settings. Using a high-content image analysis algorithm, cellular morphometric parameters and fluorescence intensities can be rapidly quantitated in an automated, unbiased, and standardized manner. Together, this approach enables informative characterization of captured cells *in situ* and potentially allows for sub-classification of circulating tumor cells, a key step towards the identification of true metastasis-initiating cells. Thus, this nano-enabled platform holds great potential for studying the biology of rare tumor cells and for differential diagnosis of cancer progression and metastasis.

Keywords

Circulating tumor cells; quartz nanowire array; laser scanning cytometry; cellomic analysis

In recent years, there has been a great surge of interest in utilizing the peripheral blood circulating tumor cells (CTCs) to predict the likelihood of cancer metastasis and monitor the therapeutic responses of patients^{1,2}. CTCs are shed by both primary and metastatic tumors and they are thought to mediate the hematogenous spread of cancer to distant sites^{3,4}. Despite the clinical and pathophysiological importance of CTCs, the utility of these cells as a cancer biomarker is limited by the availability of reliable technologies for efficient capture and functional characterization of CTCs. The difficulty resides in many aspects including

*Address correspondence to sangkwon.lee@yale.edu or rong.fan@yale.edu.

the rarity and heterogeneity of CTCs in blood. It was estimated that CTCs are present at extremely low abundance (1–100 CTCs/mL) in a noisy background of highly abundant hematologic cells ($\sim 10^9$ cells/mL) in the whole blood. To date, several technologies such as magnetic separation using immunofunctionalized magnetic beads, cell size-based mechanical separation, and microstructure-facilitated cell capture have been developed in hope to isolate, detect, and count CTCs.^{5–14} Recent reports on cell-nanostructure interaction have shown that nanometer scale topography influences not only diverse cell behavior such as cell adhesion, motility, proliferation and differentiation,^{7,8,15–26} but also the performance (efficiency and yield) of nanostructure-based cell capture.^{27–31} For example, a silicon nanowire (SiNW) substrate coated with an antibody against epithelial cell adhesion molecules (e.g., EpCAM) exhibited high capture efficiency when employed to isolate EpCAM-positive CTCs.^{28,29} All these technological advances point to the possibility of using nanostructured substrates to capture very rare cell populations including CTCs. To meet the stringent criteria of clinical CTC analysis, it is required to develop rapid quantitation of CTCs in an automated manner. Moreover, owing to the low numbers of CTCs one can separate from clinical specimens and the inherent heterogeneity of these cells, it is of vital importance to comprehensively characterize the functions of captured CTCs *in situ* in order to distinguish CTC subtypes or even metastasis-initiating cells. This is such a paramount endeavor to promote the current CTC analysis technologies to the stage of clinical utilization of CTCs as fluid biopsies for cytopathological examination and differential diagnosis of cancer metastasis.

Laser scanning cytometry (LSC) emerges as a powerful technology for high-content, high-throughput quantitative analysis of cellular functions in a fully automated manner^{32,33}. It utilizes large-area fluorescence imaging scheme and rigorous image quantitation algorithms to enable informative analysis of cell samples attached to a solid substrate, making it more amenable to the study of heterogeneous cell populations. Using either morphometric or proteomic analysis, one can generate a suite of quantitative metrics to comprehensively characterize all single cells immobilized on the substrate. While this technology represents a powerful approach for high content screening using cell lines, it has not been applied to the study of rare cells in clinical specimens, which is challenging because it lacks the capability of rare cell capture and separation.

Herein, we integrate nanowire substrate that serves as an efficient cell capture tool and laser scanning cytometry that works for quantitative, automated characterization of captured rare cells to yield an integrated, nano-enabled platform for informative analysis of CTCs. In order to capture very rare tumor cells in clinical blood samples (several tumor cells per mL), large volumes of clinical samples (\sim mL) need to be examined, for example, by flowing through a microfluidic cell capture apparatus to isolate and enrich circulating tumor cells⁹ a. Using the nanowire substrate-based imaging cytometry, we can directly apply large volumes of blood samples onto a large-area nanowire substrate, which can be imaged by laser scanning cytometry for accurate identification of all tumor cells. We also conducted informative morphometric analysis of all tumor cells captured on the substrate using high-content image analysis algorithms. When fluorescence-labeled antibodies were used to measure cell surface markers or cytoplasmic signaling proteins, it could also yield proteomic profiles of single tumor cells in hope of identifying molecular signatures and signaling pathways for CTC sub-classification. Such technology integration is not trivial. It aims to bridge the gap between prototype technology and clinical use in order to facilitate the translation of a promising nano-enabled rare cell analysis platform to diagnosis and stratification of metastatic cancers.

Fabrication and functionalization of transparent quartz nanowire arrays

The fabrication procedure for the transparent quartz nanowire (QNW) arrays is illustrated in Figure 1. It went through a series of processes including nanoparticle coating, metal deposition, pattern transfer, and deep reactive ion etching to generate vertical nanowires. Polystyrene nanoparticles (PS NPs) were applied onto a quartz wafer using either spin-casting or dip-coating. The resulting pattern exhibits short-range ordering in a close-packed manner. The size of the PS NPs can be further shrunk using oxygen plasma etching. Then these particles served as a template to deposit chromium metal forming a nanohole pattern that was inverted to yield a nanodot pattern using nickel deposition and selective chrome etching. Finally, the nanodot pattern was transferred down to the quartz substrate using oxide reactive ion etching, producing an array of quartz nanowires. The typical diameter and length are ranging from 80 to 100 nm and 250 to 350 nm, respectively (Figure 1f). The QNW array substrate is completely transparent and suitable for optical examination (both phase-contrast and fluorescence) of captured tumor cells.

The nanowire substrate was then functionalized with monoclonal anti-human EpCAM antibody using a streptavidin-immobilization method³⁴ (Figure 1g). During this procedure, as-prepared quartz nanowires were treated with oxygen plasma to render a surface with high density of silanol group. Then we applied (3-aminopropyl)-triethoxysilane (APTES) to aminate the nanowire surface, which can be further functionalized with streptavidin(STR) via a two-step aldehyde/amine reaction and using glutaraldehyde (GA) as the linker. Finally, biotinylated anti-human EpCAM was introduced to the STR-functionalized nanowires, which, through the high affinity biotin-streptavidin binding, yielded a immunofunctionalized nanowire surface coated with anti-human EpCAM antibodies. EpCAM is a pan-epithelial cell surface marker and presumably EpCAM+ cells captured from blood are carcinoma cells shed into the blood stream.

Automated imaging and quantitation of tumor cells captured on nanowire substrates

In order to accurately count and characterize very rare tumor cells such as CTCs with good statistic power, large quantities of blood samples need to be analyzed per individual patient, suggesting the need of large-area nanowire substrates ($>1'' \times 1''$) to handle the large volume of sample and ensure high-yield capture of CTCs. However it is not reliable for clinicians to perform counting or characterization of captured cells over such a large area using a conventional hemocytometer method. Here we exploited a rapid laser scanning cytometry approach to automatically quantitate all single cells captured on the substrate using a simple microarray scanner. Two laser beams (635nm and 532nm) were employed to measure fluorescence-stained tumor cells (see Supporting Method).³⁵ This approach can be fully automated and standardized for the use in clinical laboratories.

To evaluate cell capture and imaging capability, we first conducted a set of experiments using pure tumor cell samples. Cell suspensions were prepared at densities (A549, human lung carcinoma cells) ranging from ~200 to 4,300 cells per test sample (100 μ L) onto a set of PDMS microwells assembled on EpCAM functionalized QNW arrays. Figure 3a shows scanned images of A549 tumor cells captured on an anti-human EpCAM-functionalized QNW substrate as well as quantitative analyses of cellular parameters. The first and second columns show original fluorescence images and the third column shows the result of automated identification of cell shape (cell boundary shown in green) for morphometric analysis. In our experiments, we were able to simultaneously extract a dozen physical parameters and in Figure 3a (the fourth and fifth columns) we show two parameters for all single tumor cells we captured – one is the cell size and the other is cell circularity. It was

found that the average size of immobilized A549 cells was $\sim 176.3 \pm 133.3 \mu\text{m}^2$, which is in good agreement with the estimation using epifluorescence imaging (Figure S1). Cell circularity analysis indicates that most as-captured cells are round with a typical roundness factor ~ 0.88 . The observed homogeneity of morphometric parameters in all single tumor cells are what we expected because the same cell line was used in all these experiments. However, CTCs from patients are expected to be highly heterogeneous and the capability for multiparameter functional (including morphometric) analysis is useful for distinguishing CTC subsets and differential diagnosis.

We also performed A549 tumor cell capture using anti-EpCAM functionalized flat glass substrates and the results are shown in Figure S2. Then we conducted a quantitative comparison of tumor cell capture efficiency between these two platforms and at varying cell densities (Figures 3b–c). The result from nanowire substrates shows a nearly linear correlation between the number of captured cells vs loaded cells for up to 4,000 cells ($n=3$, $R^2=0.94$). The flat glass platform yields a lower regression, of approximately 0.75, than that of nanowire arrays, which indicates a higher cell-substrate interaction on nanowire arrays as compared to the flat glass substrate. This result is consistent with prior reports.^{20,21} Figure 3c shows the cell capture yield, which is defined as the percentage of captured cells to all cells initially loaded. It was found that the capture yield remains relatively constant over the wide range of cell density. The nanowire substrate gives rise to substantially higher yield than the flat glass substrates.

In order to image small numbers of tumor cells captured on nanowire arrays, we added human lung cancer cells (A549) pre-labeled with Dil (invitrogen) to culture medium with nominal cell numbers ranging from 10 to 64 per test well (100uL). Figure 3d shows the representative scanned images of two microwells. The number of loaded cells in each test well is shown in red at the lower right corner while the number of captured cells shown in yellow at the upper right corner. The average capture yield is $\sim 65.1.0 \pm 25.2\%$ (Figures 3e and f). These results demonstrated that we can accurately count captured cells using the imaging cytometry approach when the cell number is very low.

Quantitation of rare tumor cells from mixed cell populations

Here we take one step further to assess the utility of nanowire substrate-based laser imaging cytometry for CTC analysis in the settings close to clinical diagnosis – capture from mixed cell populations that can mimic patient specimen to some extent. Lung cancer cells (A549) were spiked at varying cell densities into the suspensions of human peripheral blood mononuclear cells (PBMCs) to perform tumor cell capture experiments. We also studied the mixed cell populations by spiking A549 cells to human monocytic cells (U937) (Figures S3 and S4). As shown in Figure 3a, the first and the second columns show single channel scanned images of all cells captured in a representative microwell loaded with the mixture of A549 cells and PBMCs. Tumor cells were pre-stained with green membrane dye Dil and all PBMCs pre-stained with red membrane dye DiD. The third column is the overlay of both channels. The histogram showing the quantitative image analysis of cell size distribution indicates tumor cells ($\sim 20\text{--}40\mu\text{m}$) are generally larger than PBMCs ($\sim 5\text{--}15\mu\text{m}$), manifesting the potential utility of single cell morphometric analysis for distinguishing heterogeneous cell populations. Next we systematically studied the effect of background cells on the capture yield and purity by varying the ratio of tumor and background cells. U937, a human monocytic cell line, was used as the background cells. The result indicates the capture yield of target cells (tumor cells) is relatively constant whereas the background cells do show elevated non-specific capture with increasing their density (Figure 3b and Supporting Figures S8 and S9). Finally we demonstrated the capture of rare tumor cells spiked in PBMCs at a density equivalent to clinical cancer patient samples. In this

experiment, the entire chip containing 18 PDMS microwells was used to measure one sample. Automated imaging cytometry can visualize the whole chip and rapidly identify the total number of tumor cells captured from all the microwells. Figure 3c shows the raw scanned fluorescence images of each microwell (labeled 1–18) after cell capture experiment and the tumor cell capture yield is 9 out of 15 cells spiked in the PBMC sample, demonstrating the applicability of our technology for quantitation of rare tumor cells from heterogeneous cell samples.

Human whole blood samples to assess the utility for clinical CTC analysis

We used fresh whole blood samples from two volunteers and two brain tumor patients to assess the utility of our technology for quantitative analysis of rare tumor cells by spiking ultra-low abundance A549 cells in whole blood (several A549 cells per mL of blood). These spiked samples are almost identical to the blood samples from metastatic cancer patients. The experiment procedure is the following. First, these whole blood samples were spiked with A540 cells at a level of ~10 cells per mL. Second, RBC-lysis solution was added to the spiked whole blood samples and incubated for 10 min at room temperature to remove red blood cells that may complicate fluorescence imaging. Third, the remaining cells were spun down to remove debris and re-suspended in the same volume of medium for cell capture experiment. Fourth, these samples containing rare tumor cells (~ 7 or 15 cells per mL) was introduced onto the entire nanowire substrate chip, on which there are 18 PDMS wells and each contains ~ 60 μ L of sample. The total volume of blood analyzed using a nanowire substrate is $18 \times 60 = 1,080 \mu\text{L}$ or ~1mL. Cells were incubated on the nanowire array for 30–60min for cell capture followed by a rinsing step. For each sample, we also measured unspiked blood for negative control (Figure S7). Finally, all the captured cells were fixed by 4% PFA in PBS buffer, stained with Phycoerythrin(PE)-conjugated anti-cytokeratin and YO-PRO-1 for 30 min at room temperature. Afterwards, captured cells were imaged using laser scanning cytometry to obtain cell count, cell size, shape, fluorescence intensity of each cell over the entire substrate (Figures S5 and S6).

Figure 4a shows the scanned images of all the microwells used to analyze a human blood sample (volunteer V1) using PE-conjugated anti-cytokeratin, whereas Figure 4b is the raw images for negative control (no tumor cells spiked). Figure 4c summarized the quantitative counts of captured tumor cells from all four human blood samples (P1, P2, V1 and V2) as well as from a negative control sample. Then we can determine the capture yield for these whole blood samples spiked with low-abundance tumor cells (Figure 5a) and the average capture yield is $\sim 67.5 \pm 15.0\%$. This result indicates a greater performance as compared to previous stationary nanowire-based CTC capture presumably due to the large-area of nanowire substrate and large-scale imaging capability. The imaging cytometry approach also allows for rapid quantitation of cellular parameters such as cell size (Figure 5b). Apparently the size distribution is similar for these samples, which is as expected because the same type of tumor cells (A549) were used in all the human blood sample experiments. Finally, we almost could not detect tumor cells from negative control samples according to the fluorescence signal. Only in one of all the negative control samples we observed a false signal (Figure 4b). However quantitation indicates the size of that “tumor cell” is much larger than others (Figure 5b) suggesting that imaging cytometry-based morphometric characterization may help remove false positive signal and more accurately quantitate tumor cells.

In summary, we report on a nano-enable technology platform for high-yield capture and rapid analysis of rare cells by integrating biofunctionalized quartz nanowire arrays and laser scanning cytometry. We demonstrated it can successfully capture and characterize rare tumor cells (several cells per mL) from mixed cell populations or even human whole blood,

which fully justified the utility of this technology in clinical settings. This approach can also be applied to a variety of cytopathological examinations of rare cells such as tumor stem cells from tissue biopsies and immune cell subtypes for informative immune monitoring. Using a high-content imaging cytometry approach, we show not only rapid counting of captured tumor cells but also quantitative analysis of functional parameters such as cell shape and circularity at the single cell level. It has been reported that nanostructured substrates can alter cellular behavior such as adhesion, spreading and migration^{36–38}. We performed capture of tumor cells on nanowire substrate and found size and morphology of A549 cells on quartz nanowire substrates were generally smaller and more rounded (less spreading) than the cells captured on smooth substrate (i.e. glass). (see Figure S10, Supporting Information), indicating that nanoscale topographic features do influence the cell capture and spreading. This is an interesting biological phenomenon, but also means that we need to be cautious when we interpret the morphometric signatures of captured tumor cells in hope to identify CTC subtypes. In addition, it could be exploited to analyze other functional parameters such as surface receptor expression and intracellular signaling proteins using immunocytochemistry, further enhancing the power of this integrated approach for distinguishing phenotypic diversity and functional heterogeneity of rare cells in hope of detecting the stem-like, metastasis-initiating circulating tumor cells from patients.

Supplementary Material

Refer to Web version on PubMed Central for supplementary material.

Acknowledgments

This study was supported by the U.S. National Cancer Institute Howard Temin Pathway to Independence Award (NIH 4R00 CA136759-02, PI: R.F.), the Priority Research Centers Program and by Basic Science Research Program through the National Research Foundation of Korea (NRF) funded by the Ministry of Education, Science and Technology (2010-0029706 and 2010-0019694, PI S.K.L.) and also partially supported by the Alzheimer's Association New Investigator Research Grant (PI: R.F.) and a grant from the KRIBB Research Initiative Program. S.K.L. was supported by the Visiting Professor Program (2011) from the LG-Yonam foundation while visiting the Biomedical Engineering Department of Yale University. Y.W. is supported by the Anderson Postdoctoral Fellowship. S.K.L. thanks Dr. H. Lim for initial quartz samples for the experiments and the fruitful discussion.

References

1. Yu M, Stott S, Toner M, Maheswaran S, Haber DA. *Journal of Cell Biology*. 2011; 192:373–382. [PubMed: 21300848]
2. Pantel K, Brakenhoff RH, Brandt B. *Nature Reviews Cancer*. 2008; 8:329–340.
3. Chaffer CL, Weinberg RA. *Science*. 2011; 331:1559–1564. [PubMed: 21436443]
4. Gupta GP, Massagué J. *Cell*. 2006; 127:679–695. [PubMed: 17110329]
5. Smerage JB, Hayes DF. *British Journal of Cancer*. 2006; 94:8–12. [PubMed: 16317435]
6. Kim SI, Jung H-i. *Journal of Breast Cancer*. 2010; 13:125–131.
7. Adeegbe D, Levy RB, Malek TR. *Blood*. 2010; 115:1932–1940. [PubMed: 20040758]
8. Fujisaki H, Kakuda H, Shimasaki N, Imai C, Ma J, Lockey T, Eldridge P, Leung WH, Campana D. *Cancer Research*. 2009; 69:4010–4017. [PubMed: 19383914]
9. Nagrath S, Sequist LV, Maheswaran S, Bell DW, Irimia D, Ulkus L, Smith MR, Kwak EL, Digumarthy S, Muzikansky A, Ryan P, Balis UJ, Tompkins RG, Haber DA, Toner M. *Nature*. 2007; 450:1235–U10. [PubMed: 18097410]
10. Stott SL, Lee RJ, Nagrath S, Yu M, Miyamoto DT, Ulkus L, Inserra EJ, Ullman M, Springer S, Nakamura Z, Moore AL, Tsukrov DI, Kempner ME, Dahl DM, Wu C-L, Iafrate AJ, Smith MR, Tompkins RG, Sequist LV, Toner M, Haber DA, Maheswaran S. *Science Translational Medicine*. 2010; 2

11. Fizazi K, Morat L, Chauveinc L, Prapotnich D, De Crevoisier R, Escudier B, Cathelineau X, Rozet F, Vallancien G, Sabatier L, Soria JC. *Annals of Oncology*. 2007; 18:518–521. [PubMed: 17322541]
12. Danila DC, Heller G, Gignac GA, Gonzalez-Espinoza R, Anand A, Tanaka E, Lilja H, Schwartz L, Larson S, Fleisher M, Scher HI. *Clin Cancer Res*. 2007; 13:7053–7058. [PubMed: 18056182]
13. Cristofanilli M, Budd GT, Ellis MJ, Stopeck A, Matera J, Miller MC, Reuben JM, Doyle GV, Allard WJ, Terstappen L, Hayes DF. *New England Journal of Medicine*. 2004; 351:781–791. [PubMed: 15317891]
14. Talasz AH, Powell AA, Huber DE, Berbee JG, Roh KH, Yu W, Xiao W, Davis MM, Pease RF, Mindrinos MN, Jeffrey SS, Davis RW. *Proceedings of the National Academy of Sciences of the United States of America*. 2009; 106:3970–3975. [PubMed: 19234122]
15. Lee JY, Jones C, Zern MA, Revzin A. *Analytical Chemistry*. 2006; 78:8305–8312. [PubMed: 17165820]
16. Kapur R, GKA, Campana M, Adams T, Olson K, Jung D, Mrksich M, Vasudevan C, Taylor DL. *Biomedical Microdevices*. 1999; 2:11.
17. Feigel IM, Vedala H, Star A. *Journal of Materials Chemistry*. 2011; 21:8940–8954.
18. Jiang XY, Bruzewicz DA, Wong AP, Piel M, Whitesides GM. *Proceedings of the National Academy of Sciences of the United States of America*. 2005; 102:975–978. [PubMed: 15653772]
19. Shalek AK, Robinson JT, Karp ES, Lee JS, Ahn DR, Yoon MH, Sutton A, Jorgolli M, Gertner RS, Gujral TS, MacBeath G, Yang EG, Park H. *Proceedings of the National Academy of Sciences of the United States of America*. 2010; 107:1870–1875. [PubMed: 20080678]
20. Piret G, Galopin E, Coffinier Y, Boukherroub R, Legrand D, Slomianny C. *Soft Matter*. 2011; 7:8642–8649.
21. Kulangara K, Leong KW. *Soft Matter*. 2009; 5:4072–4076.
22. Anselme K, Davidson P, Popa AM, Giazson M, Liley M, Ploux L. *Acta Biomaterialia*. 2011; 7:1936–1937.
23. Qi S, Yi C, Ji S, Fong CC, Yang M. *Acs Applied Materials & Interfaces*. 2009; 1:30–34. [PubMed: 20355748]
24. Lim JY, Hansen JC, Siedlecki CA, Runt J, Donahue HJ. *Journal of the Royal Society Interface*. 2005; 2:97–108.
25. Curtis ASG, Casey B, Gallagher JO, Pasqui D, Wood MA, Wilkinson CDW. *Biophysical Chemistry*. 2001; 94:275–283. [PubMed: 11804737]
26. Kwon KW, Choi SS, Lee SH, Kim B, Lee SN, Park MC, Kim P, Hwang SY, Suh KY. *Lab on a Chip*. 2007; 7:1461–1468. [PubMed: 17960272]
27. Kim ST, Kim DJ, Kim TJ, Seo DW, Kim TH, Lee SY, Kim K, Lee KM, Lee SK. *Nano Letters*. 2010; 10:2877–2883. [PubMed: 20698600]
28. Wang S, Wang H, Jiao J, Chen K-J, Owens GE, Kamei K-i, Sun J, Sherman DJ, Behrenbruch CP, Wu H, Tseng H-R. *Angewandte Chemie-International Edition*. 2009; 48:8970–8973.
29. Wang S, Liu K, Liu J, Yu ZTF, Xu X, Zhao L, Lee T, Lee EK, Reiss J, Lee YK, Chung LWK, Huang J, Rettig M, Seligson D, Duraiswamy KN, Shen CKF, Tseng HR. *Angewandte Chemie-International Edition*. 2011; 50:3084–3088.
30. Kim JS, Cho JB, Park BG, Lee W, Lee KB, Oh MK. *Biosensors & Bioelectronics*. 2011; 26:2085–2089. [PubMed: 20926282]
31. Lee JH, Kim JS, Park JS, Lee W, Lee KE, Han SS, Lee KB, Lee J. *Advanced Functional Materials*. 2010; 20:2004–2009.
32. Shorte S. *Cytom Part A*. 2009; 75A:711–711.
33. Harnett MM. *Nature Reviews Immunology*. 2007; 7:897–904.
34. Kim ST, Kim DJ, Kim TJ, Seo DW, Kim TH, Lee SY, Kim K, Lee KM, Lee SK. *Nano Lett*. 2010; 10:2877–83. [PubMed: 20698600]
35. Institute, B.
36. Kim W, Ng JK, Kunitake ME, Conklin BR, Yang PD. *Journal of the American Chemical Society*. 2007; 129:7228. [PubMed: 17516647]

37. Xie C, Hanson L, Xie WJ, Lin ZL, Cui BX, Cui Y. *Nano Lett.* 2010; 10:4020–4024. [PubMed: 20815404]
38. Shalek AK, Robinson JT, Karp ES, Lee JS, Ahn DR, Yoon MH, Sutton A, Jorgolli M, Gertner RS, Gujral TS, MacBeath G, Yang EG, Park H. *Proceedings of the National Academy of Sciences of the United States of America.* 2010; 107:1870–1875. [PubMed: 20080678]

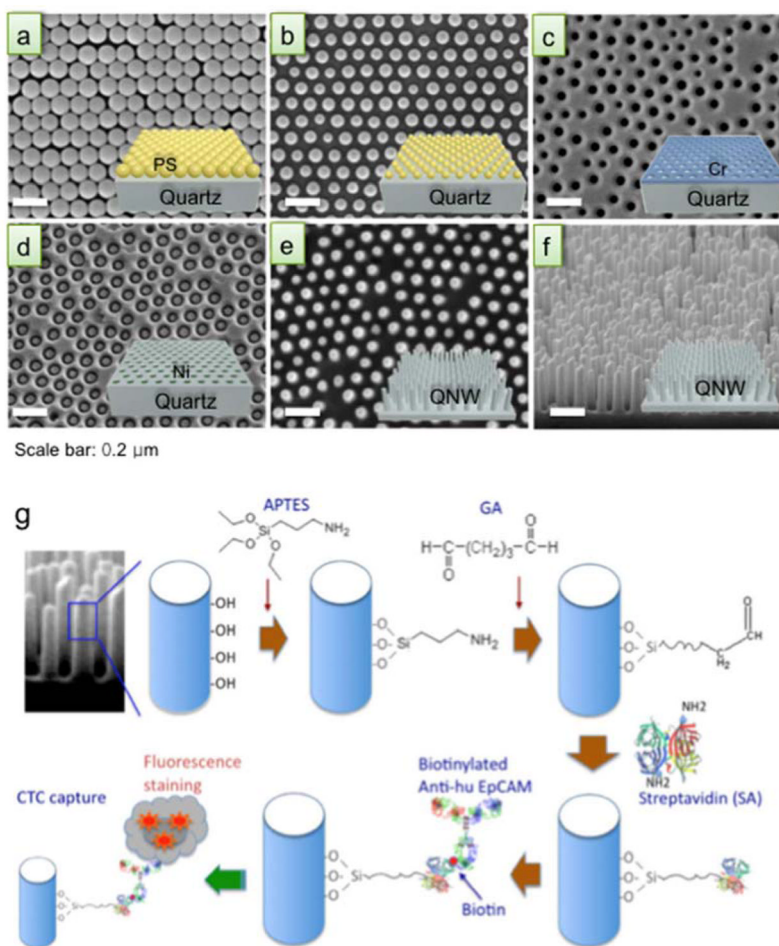


Figure 1. Fabrication and surface functionalization of quartz nanowire arrays

(a) Spin-coating process of polystyrene (PS) nanoparticles (NPs) on a flat quartz substrate. The size of the PS NPs was about 100 nm. (b) First O_2 plasma etching for size reduction of coated PS NPs. (c) Cr metal deposition (25 nm) using e-beam evaporator and lift-off of PS NPs with N-methyl-2-pyrrolidone (NMP). (d) Ni metal deposition used as an etch mask and Cr metal lift-off process. (e) and (f) Second plasma etching (top-view and tilted-view, respectively). RIE was performed to fabricate the QNW arrays with SF_4/Ar gas for 4 min. After RIE, the remaining Ni metal was completely removed with a wet-etchant (LCE-12K, Cyantek, USA). (g) Depiction of the step-by-step functionalization of nanowire surface with APTES, GA, streptavidin and biotinylated anti-human EpCAM antibody for circulating tumor cell capture.

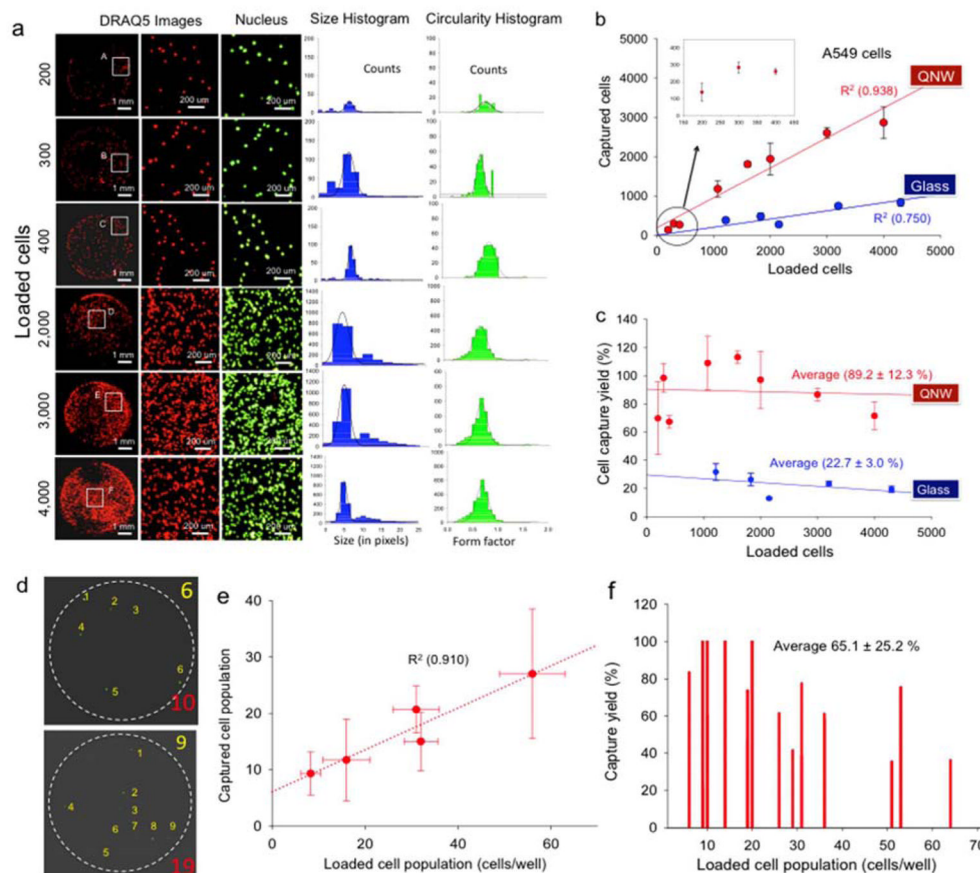


Figure 2. Imaging and quantitation of lung carcinoma cells captured on nanowire arrays

(a) First and second column: low magnification and enlarged fluorescence images (white box region shown in A, B, C, D, E, and F) of captured human lung tumor cells (A549) on STR-functionalized QNW arrays bound with PDMS wells for different loaded cell populations in the range of 200 to 4,000 cells/well. Third column: CellProfiler™ generated outlined images of captured cells on STR-QNW arrays for cell counting. Forth and fifth column: size and circularity histogram of immobilized A549 cells on STR-functionalized QNW arrays. The circularity (also known as form factor, ff), which is calculated as $[4\pi(\text{area})/(\text{perimeter})^2]$, represents the criterion of the circularity of the immobilized cells. If the form factor equals to 1, the captured object is a perfect circular object. The solid line represents a Gaussian fitting. (b) Correlation of total captured cells (A549) on STR-functionalized QNW arrays and STR-planar glass substrate versus loaded cells from cell suspension ($R^2 \sim 0.94$ and ~ 0.75 for STR-QNW and STR-planar glass, respectively). Each result and error bar represents an average with standard deviation from three repeats ($n=3$). (c) Cell capture efficiency (yield) of the captured cells (A549) on two different topographies of substrates, STR-QNW arrays and STR-planar glass substrate as a function of loaded cells in the range of 200 to 4,300 cells/well. The solid-line represents a linear fitting. Each result and error bar represents an average with standard deviation ($n=3$). (d) Representative fluorescence images of captured A549 cells (human lung tumor cells) on STR-QNW arrays with cell loading in the range of 10 to 64 cells/sample. The captured cells were pre-stained by green-Vybrant DiI and scanned by microarray scanner. The immobilized cell population was then counted manually and also compared to the images from optical and fluorescence microscopy. Yellow-colored numbers (right-top) denote the number of captured cells for each well while red-colored numbers (right-bottom) indicate the total loaded cell population.

(e) Correlation of total captured cells on STR-QNW arrays as a function of the loaded cells from cell suspension in the range of 6 to 64 cells/well, indicating a good linear relationship with the loaded cell population. The dotted line represents a linear fitting ($R^2=0.910$). Each result shows an average with standard deviation ($n=3$). (f) Cell capture yield distribution versus loaded cell population in the range of 6 to 64 cells/well.

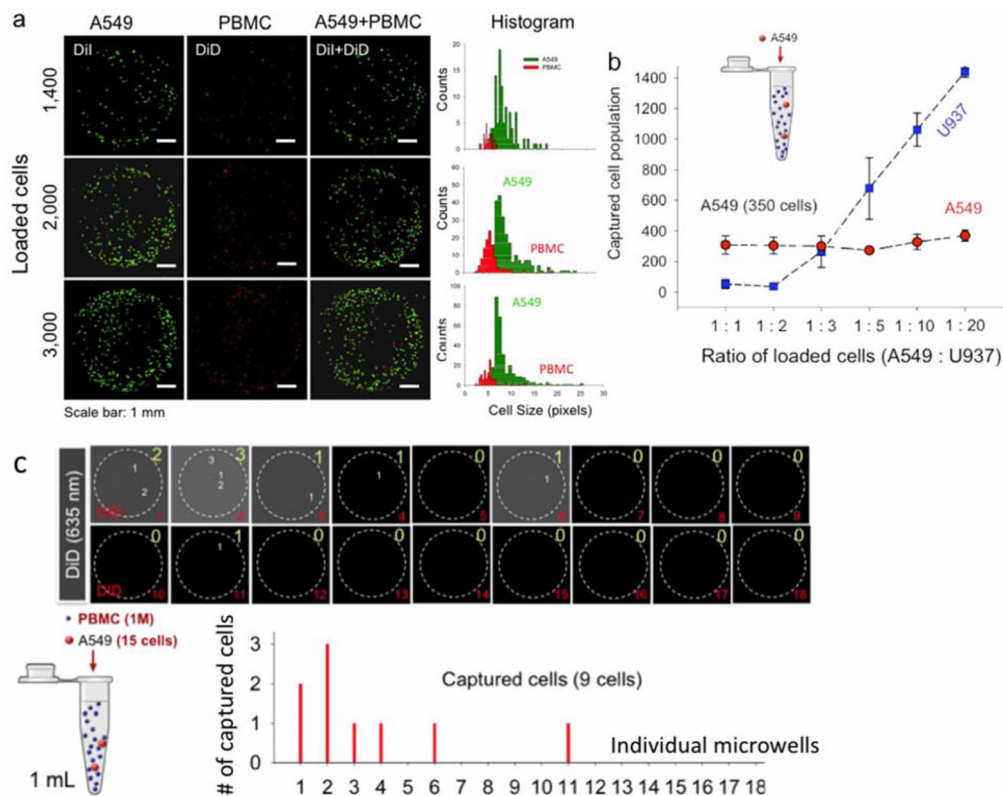


Figure 3. Capture of lung carcinoma cells from mixed cell populations

(a) Scanned images of captured cells from the mixture of A549 (green-labeled) and PBMCs (red-labeled) using nanowire arrays and the size distribution in pixels. A549/PBMC on STR-QNW arrays as a function of loaded cells in the range of 1,400 to 3,000 cells/well. (b) Both tumor cells (A549) and monocyte/background cells (U937) captured on nanowire substrate as a function of the ratio A549/U937 when the same amount of A549 cells were spiked in different densities of U93 cells. The result shows the tumor cell capture yield remains relatively constant although the non-specific capture of background cells significantly varies with the PBMC cell density. (c) Capture of rare tumor cells spiked in as-received PBMCs. Scanned images of tumor cells captured from an as-received human PBMC sample spiked with A549 lung cancer cells (15 cancer cells in 1 mL PBMC suspension). Tumor cells were pre-stained with membrane dye DiD.

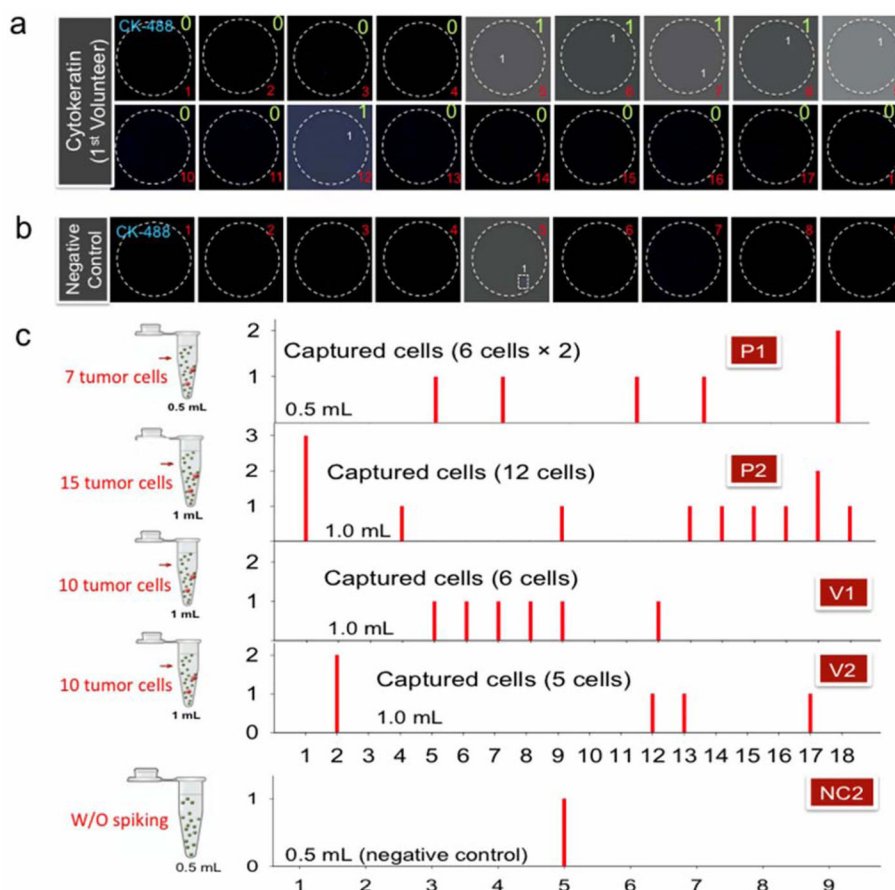


Figure 4. Capture, imaging and quantitation of lung cancer cells spiked in fresh human whole blood samples

(a) Scanned images of captured tumor cells on STR-functionalized NW substrates where only ~ 10 cells spiked into human whole blood sample. Typically, the whole blood sample (3 mL) was collected from either healthy volunteers (V1 and V2) or primary brain tumor patients (P1 and P2). 10 A549 cells were then spiked into 1 mL of RBC-lysed blood. The mock metastatic patient blood samples were evenly aliquoted and loaded into 18 microwells on top of a nanowire substrate. To identify captured CTCs from numerous other cellular components of lysed whole blood, the samples were stained with DRAQ-5 (red-665 nm) and fluorescence-conjugated anti-cytokeratin (blue-488 nm, eBioscience, USA) for all nuclei and epithelial tumor cells, respectively. Green-colored numbers (right-top) for each microarray scanned image (top of the first row) denote the number of captured cells for each well while red-colored numbers (right-bottom) indicate the microwells numbered 1 to 18. Using dual-color imaging, the tumor cells show purple (dual positive, red-DRAQ-5+/blue-CK-488+) while all the cells including non-specific cells can be identified by nuclear dye (no shown). (b) Microarray scanned images of negative control sample (as-marked NC2) from the same blood samples (V2) used for preparing spiked blood samples. (c) Summary of the captured cells for two peripheral patient samples (P1 and P2) and two volunteer blood samples (V1 and V2), showing the average capture yield to be $\sim 67.5 \pm 15\%$ ($n=4$). 10 cells of A549 (CTCs) with final volume of 1 mL were used for the capture experiments.

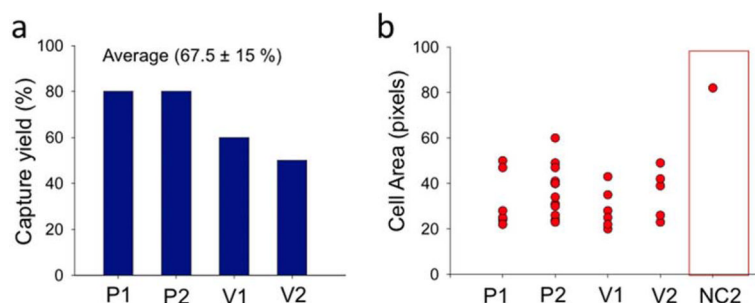


Figure 5. Quantitation and characterization of tumor cells captured from human blood samples (a) Tumor cell capture yield (the number of captured tumor cells as visualized by fluorescent marker vs. the nominal number of tumor cells spiked in 1mL of the whole blood sample). P1, P1, V1, and V2 denote samples from brain tumor patient 1, patient 2, healthy volunteers 1 and 2. (2) Cell size quantified for all captured tumor cells from four blood samples (P1, P2, V1, and V2) and one of the negative controls (NC2).